JACS
JOURNAL OF THE AMERICAN CHEMICAL SOCIETY
Article
pubs.acs.org/JACS

A Frontier Orbital Study with ab Initio Molecular Dynamics of the Effects of Solvation on Chemical Reactivity: Solvent-Induced Orbital Control in FeO-Activated Hydroxylation Reactions

Leonardo Bernasconi*[,†] and Evert Jan Baerends*[,‡,§,⊥]

[†]STFC Rutherford Appleton Laboratory, Harwell Oxford, Didcot, OX11 0QX, United Kingdom
[‡]Theoretical Chemistry Section, Vrije Universiteit Amsterdam, De Boelelaan 1083, 1081 HV Amsterdam, The Netherlands
[§]WCU program at Department of Chemistry, Pohang University of Science and Technology, Pohang 790-784, South Korea
[⊥]Chemistry Department, Faculty of Science, King Abdulaziz University, Jeddah 21589, Saudi Arabia

Supporting Information

ABSTRACT: Solvation effects on chemical reactivity are often rationalized using electrostatic considerations: the reduced stabilization of the transition state results in higher reaction barriers and lower reactivity in solution. We demonstrate that the effect of solvation on the relative energies of the frontier orbitals is equally important and may even reverse the trend expected from purely electrostatic arguments. We consider the H abstraction reaction from methane by quintet $[EDTAH_n{\cdot}FeO]^{(n-2)+}$, ($n$ = 0−4) complexes in the gas phase and in aqueous solution, which we examine using ab initio thermodynamic integration. The variation of the charge of the complex with the protonation of the EDTA ligand reveals that the free energy barrier in gas phase increases with the negative charge, varying from 16 kJ mol^{-1} for $[EDTAH_4{\cdot}FeO]^{2+}$ to 57 kJ mol^{-1} for $[EDTAH_n{\cdot}FeO]^{2-}$. In aqueous solution, the barrier for the +2 complex (38 kJ mol^{-1}) is higher than in gas phase, as predicted by purely electrostatic arguments. For the negative complexes, however, the barrier is lower than in gas phase (e.g., 45 kJ mol^{-1} for the −2 complex). We explain this increase in reactivity in terms of a stabilization of the virtual 3σ* orbital of FeO^{2+}, which acts as the dominant electron acceptor in the H-atom transfer from CH_4. This stabilization originates from the dielectric screening caused by the reorientation of the water dipoles in the first solvation shell of the charged solute, which stabilizes the acceptor orbital energy for the −2 complex sufficiently to outweigh the unfavorable electrostatic destabilization of the transition-state relative to the reactants in solution.

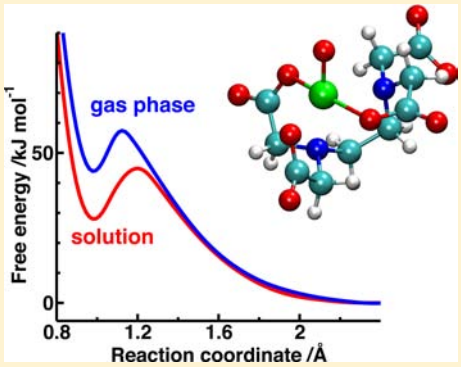

INTRODUCTION

Reaction rates for charged reactants are typically much higher in the gas phase than in solvents.[1] The change of the double-well potential in, e.g., S_N2 reactions, with minima at both the reactant and product complexes, to a unimodal energy profile with a single maximum at the transition state (TS), is perhaps the best known example. This change can be explained in terms of a selective stabilization of the reactants in solution relative to the TS: the solvation energy is larger for the reactants than for the TS, therefore the reaction barrier in solution increases.[2−11] The reason for this differential solvation effect is the fact that the reactant is typically smaller—it could for instance be a simple anion like OH^- or Cl^- in a S_N2 substitution reaction or an E2 elimination reaction—than the TS. In the TS, the negative (or positive) charge of the reactant diffuses over a larger moiety, so that the solvation energy gain is smaller.

In this paper we demonstrate that such an explanation in terms of purely electrostatic effects may be gravely incomplete. Reactivity is, apart from the effects of the charge distributions of the reactants on the energy and path of approach of the reactants (charge control), primarily governed by the (relative) energies and the character of the frontier orbitals (orbital control), which determine which bonds can be broken or formed during the reaction and how easily bond breaking/forming can occur. Therefore, a rationalization of reactivity patterns must take into account the energies and shapes of the frontier orbitals. It is crucial that also the effect of solvation on the frontier orbitals is explicitly taken into consideration. We will demonstrate here the importance of this effect in a typical case study of a C−H hydroxylation reaction of an alkane (we take methane as prototype) by an ironoxo group, the ferryl ion $Fe^{IV}O^{2+}$, with ethylenediaminetetraacetate ion $[(O_2CCH_2)_2NCH_2CH_2N(CH_2CO_2)_2]^{4-}$ ($EDTA^{4-}$, Figure 1), as a pentadentate ligand of Fe. This is an acid−base reaction where the C−H bonding orbital transfers electrons to an unoccupied low-lying σ* orbital of the FeO^{2+} group. This reaction is well studied and of major current scientific and technological importance, as briefly summarized below. It also constitutes an interesting example of a hydrogen atom

Received: November 13, 2012
Published: May 1, 2013

   dx.doi.org/10.1021/ja311144d | J. Am. Chem. Soc. 2013, 135, 8857−8867

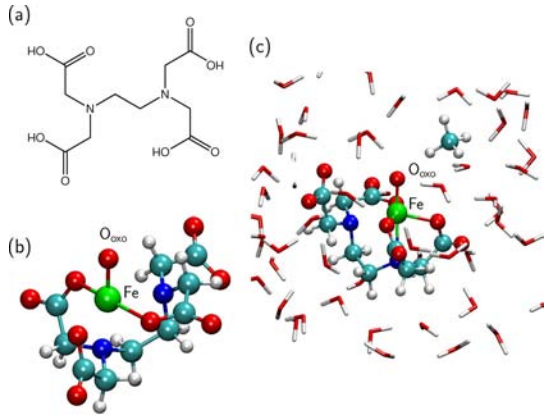

Figure 1. (a) Chemical structure of the (four times protonated) neutral EDTA ligand. (b) Sample gas-phase structure of the fully deprotonated $[EDTA{\cdot}FeO]^{2-}$ complex, from an AIMD simulation at T = 298 K. (*c*) Setup for the calculation of reaction barriers for H abstraction from methane in solution in the presence of $[EDTA{\cdot}FeO]^{2-}$. The figure shows a portion of the periodic supercell used in the calculations. The methane molecule is visible near the upper right corner, with one of the C−H bonds pointing toward the O_{oxo} atom.

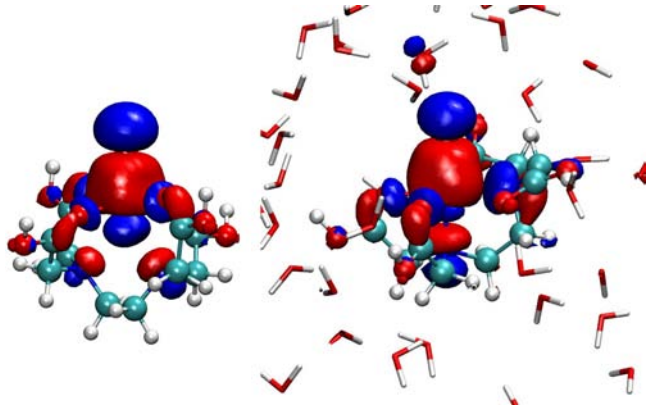

Figure 2. Isosurface at ±0.025 Å^{-3} of the 3σ* orbital of $[EDTAH_4{\cdot}FeO]^{2+}$ in the gas phase (left) and in aqueous solution (right). Both atomic configurations are taken from AIMD simulations at 298 K.

transfer[12−17] (HAT) reaction involving a substrate (in our case a methane molecule) and the oxygen atom of a (chelated) ferryl ion. We consider this reaction because the charge on the iron complex can be systematically increased by protonating the EDTA ligand along the series $[EDTAH_n]^{-4+n}$, with n = 0−4. This will allow us to separate and characterize electrostatic and orbital effects at a quantitative level.

The generation of ferryl compounds of composition $[EDTAH_n{\cdot}FeO]^{(n-2)+}$ has been postulated in kinetic and mechanistic studies of oxidation of organic compounds in aqueous Fe(0)/O_2/EDTA solution at room temperature and pressure[18−24] and confirmed by density functional theory (DFT) calculations[22−24] and ab initio molecular dynamics (AIMD) simulations.[25] These theoretical studies have also indicated that, in the gas phase, the fully protonated $[EDTAH_4{\cdot}FeO]^{2+}$ complex performs the H abstraction from methane with an enthalpy barrier of only 10 kJ mol^{-1}, potentially making this system at least as reactive as the Fenton catalyst. Similar to other quintet FeO^{2+} catalysts, the reactivity of FeO^{2+}/EDTA as an electrophilic species is dominated by the presence of a low-lying 3σ* orbital (Figure 2). This leads to an important difference in reactivity for the differently charged complexes in the gas phase. Positive charge tends to enhance the electrophilic character of the ferryl group by lowering the energy of the 3σ* acceptor, whereas the opposite holds for negative complexes. This charge effect alone may result in changes of activation enthalpy barriers for H-atom abstraction from small hydrocarbons in the gas phase of more than 10^2 kJ mol^{-1}, when going from overall +2 for n = 4 (lowest barrier) to −2 for n = 0 (highest barrier).[22]

On the basis of purely electrostatic considerations, the effect of solvation by a polar solvent on these systems is expected to be similar irrespective of the negative or positive charge of the complex: lower reactivity is predicted for an aqueous complex relative to the gas phase, since in all cases (except the neutral system) the bare complex is more strongly solvated than the TS (which contains the complex itself and a substrate CH_4 molecule). When one considers the frontier orbital aspect of this reaction, however, an important difference in the solvent effects on the reactivity is observed for systems with different charges. For the positively charged complexes, solvation takes place with the closest water molecules orienting the negative end of their dipole vector toward the complex. As we will show, the orientation of the water dipoles creates a field that destabilizes the low-lying 3σ* orbital, making the FeO^{2+} complex a less efficient electron acceptor than its gas-phase counterpart. In this case, electrostatic and orbital effects both contribute to making the electron transfer from the substrate less favorable. The orbital contribution, masked by the strong electrostatic destabilization of the TS, might not even be recognizable. The situation is different for the negatively charged complexes. In the gas phase these complexes have a lower reactivity than the positive complexes since, as noted, the negative overall charge destabilizes the 3σ* acceptor orbital.[22] However, solvation will now take place with the positive ends of the water dipoles oriented toward the negatively charged Fe complex. The resulting dipole field will therefore stabilize the acceptor orbital, with a consequent reduction of the (free) energy barrier for H abstraction from methane. This purely electronic effect counteracts the relative electrostatic destabilization (with respect to the bare complex) of the TS upon solvation. Depending on its magnitude, this effect can dominate over the reaction barrier increase from electrostatic effects. Our calculation will prove that the electronic effects are indeed the main component in determining the reaction barrier of the negative $[EDTA{\cdot}FeO]^{2-}$ complex, for which we observe a decrease of the reaction free energy barrier in solution compared to the gas phase. We remark that although the changes in reactivity we describe are a direct consequence of the charge-induced polarization of the local solvent environment near the solute, they cannot be understood on the basis of a classical reaction field model generating an almost uniform field on the reaction system. As we will show, a quantitative picture of these effects relies on a detailed knowledge of the effect of solvation on the orbital energy gap of the donor and acceptor orbitals.

■ COMPUTATIONAL DETAILS

Details of Calculations. AIMD simulations were performed using the hybrid Gaussian/plane-wave[26] package CP2K Quickstep[27,28] version 2.2.177. Standard double-ζ VB basis sets and Goedecker−Teter−Hutter pseudopotentials[28,29] were used for all atomic species. A cutoff of 280 Ry was used in the plane-wave expansion. Exchange−

correlation effects were described at the BLYP[30,31] level of theory. Atomic positions were propagated using Born−Oppenheimer dynamics[32] with a time-step of 0.5 fs. The simulation temperature was controlled through a Nosé−Hoover thermostat. Trajectory analysis and visualization were carried out using VMD[33] version 1.8.6 and XCrySDen[34] version 1.5.17.

The liquid solution structure was modeled within periodic boundary conditions using a cubic supercell of side a = 14.750 Å, containing one $[EDTAH_n{\cdot}FeO]^{(n-2)+}$ unit and 63 water molecules, in the presence of a homogeneous charge background to enforce neutrality (Figure 1). A similar set up has been used in previous calculations[25] and has been shown to provide a satisfactory representation of the solvent structure in the vicinity of (charged) FeO^{2+}/EDTA complexes. For the calculations on H-atom abstraction from CH_4, one of the water molecules was replaced by CH_4, while the supercell size was kept constant. The size of the supercell was calculated by imposing the zero-pressure condition at T = 298 K in classical MD simulations carried out using DLPOLY 2.[35] A Buckingham potential was used for the $Fe-O_{H_2O}$ interaction, and Lennard-Jones potentials were used for all other interactions between atoms of $[EDTAH_4{\cdot}FeO]^{2+}$ and water molecules. The solvent was described at the SPC/E level.[36] The final atomic configuration of the classical MD simulation was then used as a starting set of atomic positions for the AIMD simulations, after allowing extensive (∼50 ps) ab initio equilibration.

Calculation of Free Energies. Free energies for H-abstraction from methane were computed using standard thermodynamic integration techniques (see, e.g., ref 37). The reaction simply involves the migration of a proton from CH_4 to the O_{oxo} atom of $[EDTAH_n{\cdot}FeO]^{(n-2)+}$ and the simultaneous transfer of one electron from the highest occupied orbital of the substrate to the virtual $3\sigma^*$ orbital of the FeO^{2+} group. This process was modeled by constraining the distance between one of the methane H atoms and the O_{oxo} atom to a series of fixed values ξ_i. AIMD simulations were then performed at each value of ξ_i by solving equations of motion with the constraint imposed in the form of a Lagrangian multiplier $\lambda(\xi_i)$. The mean force of the constraint $f(\xi_i)$ was computed from the unbiased time averaged value of $\lambda(\xi_i)$ to give[38,39]

$$f(\xi_i) - f_0 = \langle\lambda(\xi_i)\rangle - \frac{2k_BT}{\xi_i} \quad (1)$$

where f_0 is the value of $f(\xi_i)$ for the largest value of $H_{CH_4}-O_{oxo}$ distance considered (ξ_0 = 2.36 Å), $k_B = 1.38 \times 10^{-23}$ J K^{-1}, and T = 298 K. Time averages were computed over a period of 5 ps, following 1 ps of equilibration for each value of ξ_i. ξ_i was varied in steps of 0.1 Å, in sequence from ξ_0 to its shortest value ξ_i = 0.936 Å. The potential of mean force (free energy) $\Delta G(\xi)$ was then estimated by numerical integration:

$$\Delta G(\xi) = -\int_{\xi_0}^{\xi} f(\xi')\mathrm{d}\xi' \quad (2)$$

To improve numerical accuracy in the integration, the $f(\xi_i)$ vs ξ_i profiles obtained from eq 1 were smoothed using spline curves with increments $\delta\xi$ = 0.003 Å.

THE H ABSTRACTION REACTION FROM METHANE CATALYZED BY FEO/EDTA COMPLEXES

The systems chosen for this study, the $[EDTAH_n{\cdot}FeO]^{(n-2)+}$ (n = 0−4) series of complexes, are of great interest in their own right. The remarkable catalytic activity of oxidoiron(IV) (ferryl) compounds in the hydroxylation of poorly reactive hydrocarbons has indeed been the subject of sustained experimental and theoretical scrutiny for over 40 years.[40−57] The last two decades have witnessed a further surge of interest, which has led to a number of important milestones, including: (1) the identification of the hydrated ferryl ion, $[(H_2O)_5{\cdot}FeO]^{2+}$, as the main active species in oxidation reactions catalyzed by the Fenton mixture (aqueous ferrous salts and hydrogen peroxide) in various experimental conditions;[58−66] (2) the characterization of ferryl-based key intermediates in the catalytic cycles of several enzymatic complexes, including taurine α-ketoglutarate dioxygenase (TauD)[67] and soluble methane monooxygenase (sMMO);[68−87] and (3) the synthesis and spectroscopic characterization of stable inorganic FeO^{2+} complexes with moderately high C−H activation ability.[88−99] The insight gathered in these studies is of great technological relevance, in view of the potential application of FeO^{2+}-based catalysts in the conversion of saturated hydrocarbons at ambient conditions for the production of fuels (e.g., methanol from the direct oxidation of methane)[100] or for further chemical processing.

Despite the variety and complexity of the chemical processes involved in C−H bond activation by ferryl systems, a few unifying concepts have emerged that account for the main characteristics of the reactivity of the ferryl ion, both in vivo and in inorganic environments. For example, it has been found that the ability of the FeO^{2+} moiety to activate strong C−H bonds is associated with the presence of low-lying empty acceptor orbitals with a lobe on the O atom.[66,99,101−107] This orbital acts as an acceptor of electrons from the C−H substrate in the first step of the rebound mechanism of C−H activation.[52,53,57] In particular systems with a high-spin quintet ground state are active, which can be explained in frontier orbital terms from the special stabilization of the empty $3\sigma^*$ orbital in the strong exchange field of the high-spin electrons.[66,101,105] An explanation can also be given in terms of exchange stabilization of a high-spin TS.[108,109] The stabilization of the $3\sigma^*$ orbital in the quintet state will favor the "σ-channel" (attack by the nucleophile at the up-spin $3\sigma^*\alpha$ acceptor orbital) over the "π-channel" (attack at the down-spin $\pi^*\beta$ acceptor orbital).[101,107,110] For this reason, systems involved in the direct oxidation of saturated substrates, e.g., $[(H_2O)_5{\cdot}FeO]^{2+}$ in the Fenton mixture, the two FeO^{2+} units in the Fe(IV)Fe(IV)-bis-μ-oxo "diamond-core" active center of sMMO (which effects the conversion of methane into methanol) and the [2-His, 1-carboxylate] site of the catabolic enzyme TauD[111,112] are invariably in a quintet state. By contrast, FeO^{2+} intermediates involved in biosynthesis or energy transfer, like the heme Fe a_3 site of cytochrome c oxidase,[113−116] along with the majority of the synthetic ferryl complexes synthesized to date, all possess a lower spin (triplet) state. In the triplet state, the $3\sigma^*$ orbital is substantially destabilized, and it plays virtually no role, which effectively results in a much reduced electrophilic character. The spin multiplicity of the FeO^{2+} group is determined almost exclusively by the nature of the local coordination environment. In the presence of weakly coordinating donor groups (e.g., oxygen-based) the quintet state is preferred, whereas stronger (e.g., nitrogen-based) donors favor the triplet.[105] This rule applies equally to biological and inorganic systems and makes it possible to predict the overall spin state of a ferryl complex on the basis of the structure of the ligand environment alone.

A major advantage of FeO^{2+}/EDTA complexes over the Fenton catalyst is that their generation occurs via direct reduction of atmospheric dioxygen at room temperature through a (slightly modified[25]) van Eldik mechanism.[117−119] According to recent studies based on AIMD and ab initio metadynamics, the O_2 activation occurs through the intermediate formation of a dinuclear complex (e.g., [EDTAH·FeO·O-Fe·EDTAH]$^{2-}$ in the case of the singly protonated EDTA ligand), both in gas phase and in solution, with a strong structural resemblance to the "diamond-core" of intermediate **Q** in the catalytic cycle of sMMO.[68,69,81,95] The O_2 molecule is

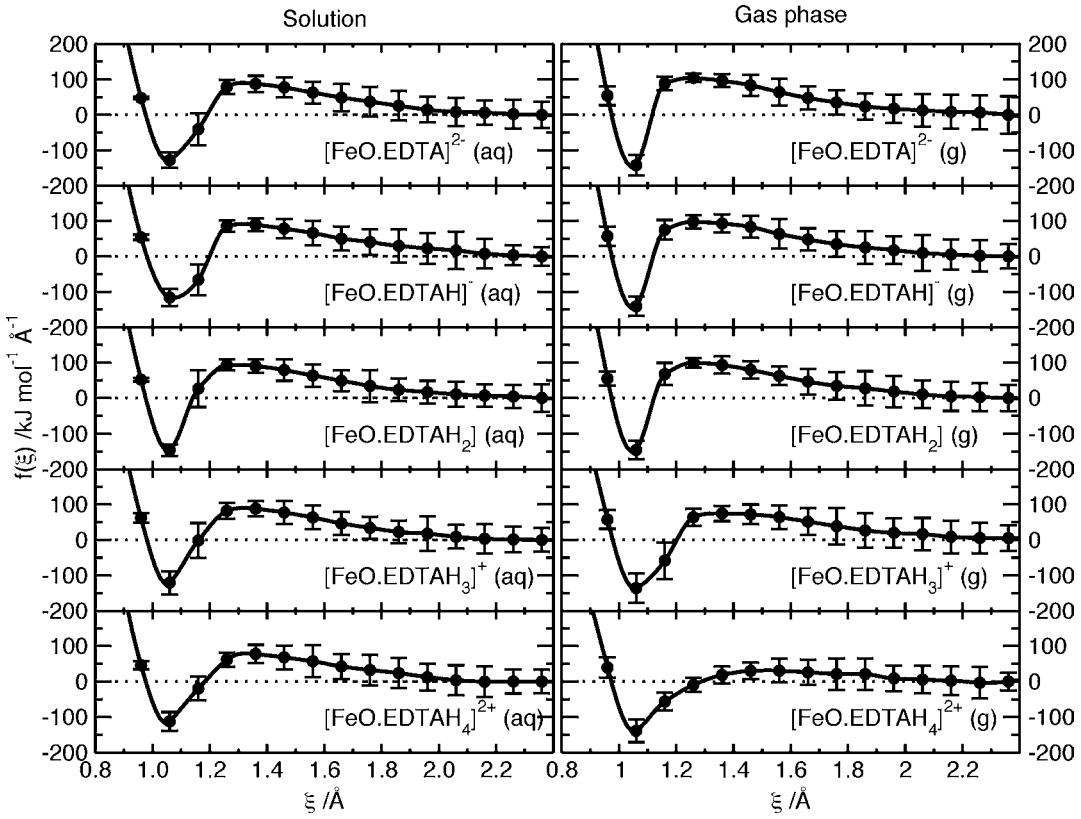

Figure 3. Mean force of constraint $f(\xi)$ as a function of the constraint value ξ for H-atom abstraction catalyzed by $[EDTAH_n{\cdot}FeO]^{(n-2)+}$ in solution and in gas phase. ξ corresponds to the $H_{CH_4}{-}O_{oxo}$ distance. The dots represent the values ξ_i at which $f(\xi_i)$ was estimated using eq 1. The continuous curves are spline interpolations of ξ_i. Standard deviations for $\langle\lambda(\xi_i)\rangle$ in eq 1 are indicated by vertical bars.

Table 1. Key Bond Distances (in Å) Defining the Fe Coordination by the Oxo Ion (O_{oxo}) and by Carboxylic-Arm Oxygens O_{carb} and Nitrogens of the EDTA Ligand in the Gas Phase (gp) and in Solution (aq)[a]

	Fe−O_{oxo}		Fe−O_{carb}(1)		Fe−O_{carb}(2)		Fe−O_{carb}(3)		Fe−O_{carb}(4)		Fe−N(1)		Fe−N(2)	
complex	gp	aq	gp	aq	gp	aq	gp	aq	gp	aq	gp	aq	gp	aq
Reactants														
$[EDTAH_4{\cdot}FeO]^{2+}$	1.651	1.660	2.243	2.173	2.448	3.439	2.173	2.169	2.200	2.072	2.258	2.164	2.461	2.234
$[EDTAH_3{\cdot}FeO]^{+}$	1.667	1.669	2.417	2.269	4.023	3.855	1.897	1.977	2.238	2.148	2.200	2.164	2.262	2.226
$[EDTAH_2{\cdot}FeO]$	1.667	1.679	3.620	3.642	1.994	1.958	1.921	1.953	3.110	2.473	2.250	2.193	2.334	2.410
$[EDTAH{\cdot}FeO]^{-}$	1.670	1.676	4.417	3.996	2.065	2.060	2.008	1.973	2.082	2.184	2.238	2.194	2.593	2.304
$[EDTA{\cdot}FeO]^{2-}$	1.679	1.674	5.740	3.849	2.061	2.067	2.033	1.970	2.167	2.139	2.228	2.197	2.441	2.486
Transition State														
$[EDTAH_4{\cdot}FeO]^{2+}$	1.774	1.767	2.245	2.216	2.745	3.436	2.277	2.196	2.222	2.105	2.344	2.241	2.361	2.274
$[EDTAH_3{\cdot}FeO]^{+}$	1.796	1.764	3.973	2.199	2.454	4.085	1.911	2.001	2.311	2.132	2.252	2.219	2.285	2.327
$[EDTAH_2{\cdot}FeO]$	1.743	1.855	4.737	2.199	1.949	4.085	1.944	2.001	2.838	2.132	2.315	2.219	2.364	2.327
$[EDTAH{\cdot}FeO]^{-}$	1.747	1.785	5.408	5.332	2.055	2.137	2.040	2.041	2.035	2.098	2.302	2.348	2.479	2.380
$[EDTA{\cdot}FeO]^{2-}$	1.785	1.832	5.747	3.850	2.063	2.095	2.044	2.083	2.136	2.068	2.311	2.401	2.442	2.420
Products														
$[EDTAH_4{\cdot}FeO]^{2+}$	1.889	1.853	2.369	2.260	2.228	3.434	2.232	2.176	2.268	2.115	2.449	2.116	2.433	2.248
$[EDTAH_3{\cdot}FeO]^{+}$	1.897	1.867	5.450	2.210	2.584	4.164	2.233	2.087	2.416	2.213	2.160	2.237	2.708	2.423
$[EDTAH_2{\cdot}FeO]$	1.835	1.898	5.286	4.752	1.925	1.995	1.938	1.981	2.981	2.340	2.187	2.190	2.338	2.415
$[EDTAH{\cdot}FeO]^{-}$	1.866	1.869	5.520	5.353	1.995	2.087	1.987	1.952	2.097	2.153	2.162	2.163	2.594	2.404
$[EDTA{\cdot}FeO]^{2-}$	1.883	1.873	5.710	4.323	2.004	2.060	1.984	1.955	2.256	2.137	2.227	2.164	2.420	2.442

[a]All distances have been obtained by averaging over trajectories at fixed values of the constraint corresponding to the reactants ($\xi \simeq 2.5$ Å), the TS ($\xi_i \simeq 1.1$ Å), and the products ($\xi_i \simeq 0.9$–1 Å) of the H abstraction reaction from methane.

reduced and cleaved inside the complex, which, according to free-energy estimates from AIMD, can then dissociate spontaneously at room temperature to generate solvated FeO^{2+}/EDTA species.[25] For the purposes of this study, the $[EDTAH_n{\cdot}FeO]^{(n-2)+}$ complexes represent model systems in which the ligand charge can be systematically varied by changing the EDTA protonation number, n, to obtain a series of FeO^{2+} chelates with charges in the range +2 to −2 while

dx.doi.org/10.1021/ja311144d | J. Am. Chem. Soc. 2013, 135, 8857−8867

maintaining the structure of the complex approximately unchanged.[22] In experimental conditions, $[EDTAH_4{\cdot}FeO]^{2+}$ is stable in very acidic solutions, and lower protonation numbers can be achieved by progressively increasing the pH.[117] In the simulations described in this paper, which are based on an explicit quantum mechanical description of both the $[EDTAH_n{\cdot}FeO]^{(n-2)+}$ solute and the water solvent, pH variations are enforced by suitably constraining the protonation number of the EDTA ligand. In experimental work, it may not be desirable to work at extremely low pH, in which case replacement of the −OH groups of the carboxylic groups with F atoms or $-CH_3$ groups can be proposed, to obtain FeO chelates with hydroxylation activity comparable to FeO/EDTA systems. Such chemical modifications of the $EDTAH_n^{-4+n}$ ligands are however not the subject of the present work and will be presented elsewhere.

RESULTS AND DISCUSSION

The mean force profiles for H abstraction from methane catalyzed by the five $[EDTAH_n{\cdot}FeO]^{(n-2)+}$ complexes in the gas phase and in solution are shown in Figure 3. Positive values of $f(\xi)$ indicate that the $H_{CH_4}-O_{oxo}$ distance has a tendency to increase relative to the value imposed by the constraint. The intercept of each profile with the x axis, $\xi^{\ddagger}$, represents the TS of the H-atom transfer, $[H_3C\cdots H_{CH_4}\cdots O_{oxo}Fe]^{\ddagger}$. In the gas phase, $\xi^{\ddagger}$ decreases with decreasing charge from 1.3 Å in $[EDTAH_4{\cdot}FeO]^{2+}$ to 1.1 Å in $[EDTA{\cdot}FeO]^{2-}$. This indicates that CH_4 needs to approach the O_{oxo} atom of a negatively charged complex closer for the electron transfer to the $3\sigma^*$ acceptor to occur. As will be shown below, this fact is largely a consequence of the destabilization of the $3\sigma^*$ orbital, which reduces the electrophilic character of the FeO^{2+} group. The overall negative charge of the complex of course also contributes to hinder the electron transfer. In solution, the dependence of $\xi^{\ddagger}$ on the charge is by contrast far less pronounced, oscillating around 1.2 Å in all systems.

Key bond distances describing the coordination of the Fe ion for all systems in the gas phase and in solution, averaged over AIMD trajectories at selected values of ξ, are summarized in Table 1 (cf. also Figures 1 and 2). The "ideal" coordination of the FeO^{2+} by EDTA, evinced from optimized complex geometries in the gas phase,[22] involves at most four equatorial oxygen atoms from carboxylic groups and two nitrogen atoms roughly in axial position to the ferryl group. The bonding of the equatorial oxygens is relatively labile, and even optimized geometries at T = 0 may loose the four-fold coordination depending on the charge of the complex. The fully protonated complex adopts the most symmetric configuration. This situation is conserved in the AIMD simulations, both in gas phase and in solution. Typically, FeO^{2+} is coordinated by 3 equatorial oxygens at 2−2.5 Å, with a further oxygen at 4−5 Å, for all values of ξ. The fully protonated complex retains four-fold equatorial coordination in the gas phase at room temperature, but three-fold coordination is observed in solution, with a remote carboxylic oxygen at 3.4 Å. This situation confirms that the interaction between the carboxylic oxygens and the Fe ions is weak and easily perturbed by either finite temperature vibration of the EDTA framework or by interaction of the ligand with the solvent. Ultimately, this weakness in the FeO^{2+} equatorial coordination explains the tendency of all the FeO/EDTA complexes studied to retain a quintet ground state at all values of ξ (for a discussion of the importance of the equatorial donor strength in influencing the ground spin state of the ferryl group see, e.g., refs 22 and 105). By contrast, the coordination from the two axial nitrogens is far less affected by temperature and by the presence of the solvent. The axial ligands are responsible for fine-tuning the reactivity of the FeO^{2+} group, via a selective stabilization or destabilization of the $3\sigma^*$ orbital.[105] The relative stability of the axial coordination structure in all complexes studied here confirms that possible changes in FeO^{2+} reactivity have to be related to factors other than the local ligand environment. As we will show, the overall ligand charge and the presence of the solvent, rather than changes in the ligand structure, are indeed the dominant factors influencing the electrophilic properties of the ferryl group in these systems. Finally, we note that the $Fe-O_{oxo}$ bond length increases for all systems in going from the reactants to the products, by ∼0.3 Å. This confirms that the oxidation of methane by FeO/EDTA systems occurs through the traditional rebound mechanism,[52,53,57] whose first step entails the transfer of one electron to the $3\sigma^*$ acceptor orbital of FeO^{2+}, with a consequent reduction of the $Fe-O_{oxo}$ bond order.

The free energies profiles computed from eq 2 are plotted in Figure 4, and they show that for the +2 complex the barrier in

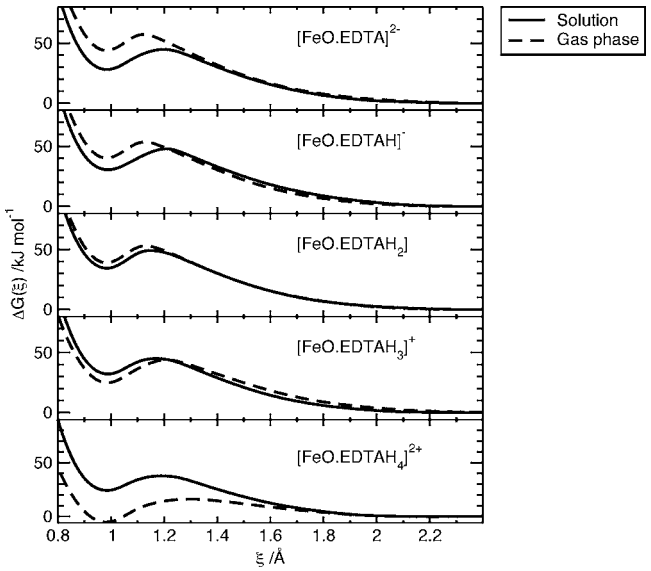

Figure 4. Free energies $\Delta G(\xi)$ for H abstraction from CH_4 catalyzed by $[EDTAH_n{\cdot}FeO]^{(n-2)+}$ in solution and in gas phase, computed from eq 2 using the data shown in Figure 3.

solution, $\Delta G_{aq}(\xi)$, exhibits the typical behavior of being higher than the corresponding gas phase value, $\Delta G_{gp}(\xi)$, whereas for the −2 complex the barrier is actually lower in solution. As the charge of the complex decreases, $\Delta G_{aq}(\xi)$ remains virtually unchanged, whereas $\Delta G_{gp}(\xi)$ increases monotonically. The two profiles are essentially overlapping for the neutral complex $[EDTAH_2{\cdot}FeO]$, whereas for negative charges, $\Delta G_{aq}(\xi) \leq \Delta G_{gp}(\xi)$ for most values of ξ. We therefore expect that the work required to carry out the H abstraction for a given complex will be higher in solution than in the gas phase for positively charged complexes, higher in the gas phase for negatively charged complexes, and about the same in the gas phase and in solution for a neutral complex.

From the free energy differences between the TS (corresponding to the maxima between 1.0 and 1.4 Å in

dx.doi.org/10.1021/ja311144d | J. Am. Chem. Soc. 2013, 135, 8857−8867

Figure 4) and the reactants, we estimated the free energy barriers of the reactions in solution and in the gas phase, $\Delta G^{\ddagger}_{aq}$ and $\Delta G^{\ddagger}_{gp}$ respectively (Table 2). As expected from the free energy profiles, $\Delta G^{\ddagger}_{gp}$ increases sharply as the charge varies from +2 to 0, and it then shows a tendency to plateauing for negative charges. The overall increase of $\Delta G^{\ddagger}_{gp}$ over the charge range +2/−2 is 41 kJ mol^{-1}. This trend mirrors the enthalpies calculated from the energy differences between the geometry optimized TS and the reactants, $\Delta H^{\ddagger}_{gp}$.[22] $\Delta H^{\ddagger}_{gp}$ varies over a wider range, from 10 kJ (+2) to 124 kJ mol^{-1} (−2). The data are summarized in Figure 5, in which we also plot the reaction entropy in the gas phase, estimated from

$$\Delta S_{gp} = \frac{\Delta H_{gp} - \Delta G_{gp}}{T} \quad (3)$$

It is interesting to observe that all complexes have comparable positive values of $\Delta S^{\ddagger}_{gp}$, with the exception of the doubly charged one, $[EDTAH_4{\cdot}FeO]^{2+}$, for which $\Delta S^{\ddagger}_{gp} \simeq 0$. This is possibly a consequence of the particularly stable structure adopted by $[EDTAH_4{\cdot}FeO]^{2+}$, in which the four carboxylic arms of EDTA are all protonated and act as neutral O-donors to Fe(IV). In all the other systems, at least one carboxylic group is negatively charged, which imbalances the symmetric arrangement of the ligand and seems to make the system more prone to distortion as the TS of the H abstraction is approached.[22] The $[EDTA{\cdot}FeO]^{2-}$ system is also symmetric in its free, gas phase geometry, but its structural stability is expected to be inferior to $[EDTAH_4{\cdot}FeO]^{2+}$, because of the presence of four negatively charged carboxylic groups in close proximity.

The trend in reactivity as a function of charge shows a remarkable correlation with the distribution of the energy of the 3σ* orbital, $p(\varepsilon^{3\sigma*})$, Figure 6. For the solvated systems, a shift of −3.5 eV has been applied in the calculation of the 3σ* orbital energies, to account for the bias in the electrostatic potential in periodic systems.[120] A large increase in the $\varepsilon^{3\sigma*}$ energy (∼4 eV) is observed in the gas phase, whereas a much reduced variation (∼1 eV) is observed in solution. Correspondingly, the ability of the FeO^{2+} group to act as an electron acceptor in the gas phase is reduced as the ligand becomes more negative, whereas it remains roughly constant in aqueous solution. In practice however, the energy of the donor orbital (HOMO of CH_4) also plays a role: the transfer of an electron to the 3σ* orbital is more favorable if the energy of the CH_4 donor orbital is higher.[22,66] Therefore, energy differences between acceptor and donor orbitals are expected to provide a better reactivity index than the acceptor orbital energy alone.

To confirm this hypothesis, we estimated the time-averaged acceptor−donor orbital energy difference for each system in gas phase and in solution. This quantity was computed by averaging over configurations obtained from AIMD at a $H_{CH_4}{-}O_{oxo}$ distance of ∼3 Å. This large value guarantees that the donor CH_4 molecule and the FeO^{2+} catalyst are experiencing comparable interactions with the environment and, at the same time, that they are at sufficiently large distance

Table 2. Activation Free Energy for H Abstraction in kJ mol^{-1} from Methane in Solution ($\Delta G^{\ddagger}_{aq}$) and in the Gas Phase ($\Delta G^{\ddagger}_{gp}$) by the Five FeO^{2+}/EDTA Complexes[a]

complex	$\Delta G^{\ddagger}_{aq}$	$\Delta G^{\ddagger}_{gp}$	$\Delta H^{\ddagger}_{gp}$	$\Delta S^{\ddagger}_{gp}$
$[EDTAH_4{\cdot}FeO]^{2+}$	38	16	10	−0.02
$[EDTAH_3{\cdot}FeO]^{+}$	45	44	99	0.18
$[EDTAH_2{\cdot}FeO]$	49	53	106	0.18
$[EDTAH{\cdot}FeO]^{-}$	48	54	123	0.23
$[EDTA{\cdot}FeO]^{2-}$	45	57	124	0.22

[a] $\Delta H^{\ddagger}_{gp}$ (from ref 22) are activation enthalpies of abstraction for the same reaction in the gas phase, computed from the differences in energy between the TS and the reactants. Activation entropies of reaction in the gas phase (in kJ mol^{-1} K^{-1}), $\Delta S^{\ddagger}_{gp}$, are estimated from eq 3.

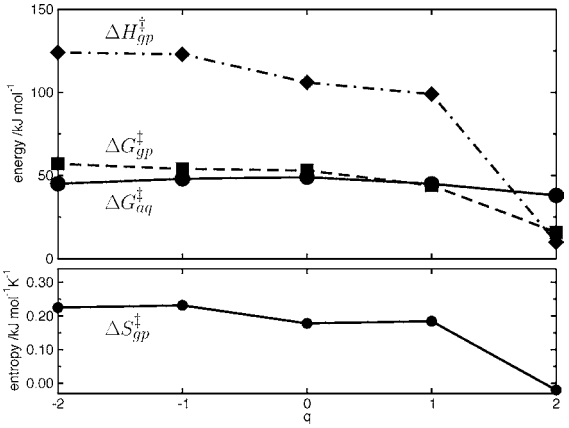

Figure 5. Dependence on the charge of the complex of the activation free energy in solution ($\Delta G^{\ddagger}_{aq}$) and of the activation enthalpy ($\Delta H^{\ddagger}_{gp}$), activation entropy ($\Delta S^{\ddagger}_{gp}$), and activation free energy ($\Delta G^{\ddagger}_{gp}$) in the gas phase, cf., Table 2.

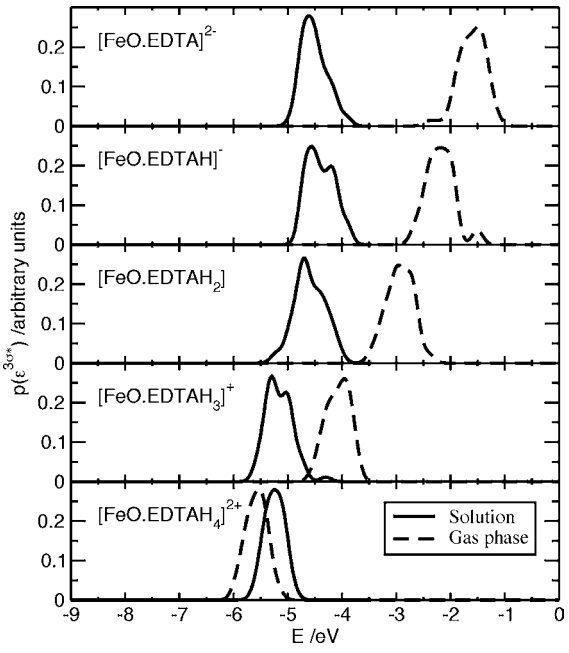

Figure 6. Distribution $p(\varepsilon^{3\sigma*})$ of the 3σ* orbital energy of FeO^{2+} averaged over 5 ps AIMD trajectories. The plots were obtained by averaging over 50 atomic configurations equally spaced along the trajectories and convoluting the resulting histograms with Gaussian functions of standard deviation 0.02 eV. A constant shift of −3.5 eV has been applied to the all energies in solution to account for the bias in the electrostatic reference for a periodic system.

dx.doi.org/10.1021/ja311144d | J. Am. Chem. Soc. 2013, 135, 8857−8867

to make direct catalyst−substrate orbital interactions negligible. The energy of the $3\sigma^*$ orbital is easy to estimate both in the gas phase and in solution as the corresponding Kohn−Sham orbital is well separated from other higher energy states. The situation is more complicated for the donor HOMO of CH_4, which, in solution, shows partial mixing with water molecules from the top of the valence band of the solvent. As a first approximation, we identified the CH_4 HOMO with the highest energy Kohn−Sham orbital ϕ_i within 3 eV of the Fermi energy for which the value of the quantity

$$S_i = \langle \phi_i | e^{-|\mathbf{r}-\mathbf{R}_C|} | \phi_i \rangle \quad (4)$$

is non-negligible. In this expression $\mathbf{R}_C$ is the position of the C atom of methane. We found that the orbital with the largest CH_4 HOMO character is typically in the range HOMO−(HOMO-5), although occasionally two or more orbitals very close in energy were found to have comparable values of S_i. In these cases, only the orbital with the largest value of S_i was taken into consideration. The acceptor−donor energy difference E_g was then simply computed from the difference between $3\sigma^*$ and ϕ_i. The time averaged values of this quantity, $\langle E_g \rangle$, are shown in Table 3 and Figure 7. The calculated values of $\langle E_g \rangle$

Table 3. Energy Differences in eV between the Acceptor $3\sigma^*$ FeO^{2+} Orbital and the Donor CH_4 HOMO in Solution (aq) and in the Gas Phase (gp) Averaged over 50 AIMD Atomic Configurations at ξ = 2.36 Å Spanning a Total Time of 5 ps[a]

complex	$\langle E_g \rangle$ (aq)	$\langle E_g \rangle$ (gp)
$[EDTAH_4{\cdot}FeO]^{2+}$	1.72 [0.20]	0.81 [0.25]
$[EDTAH_3{\cdot}FeO]^{+}$	1.38 [0.23]	1.35 [0.28]
$[EDTAH_2{\cdot}FeO]$	1.77 [0.28]	1.80 [0.19]
$[EDTAH{\cdot}FeO]^{-}$	1.51 [0.19]	1.72 [0.19]
$[EDTA{\cdot}FeO]^{2-}$	1.52 [0.30]	2.05 [0.16]

[a]Values in square brackets are standard deviations. See also Figure 7.

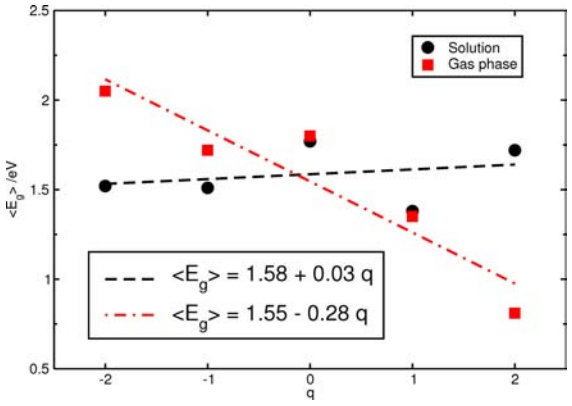

Figure 7. Energy differences between the acceptor $3\sigma^*$ FeO^{2+} orbital and the donor CH_4 HOMO in solution and in the gas phase, averaged over 5 ps at ξ = 2.36 Å, cf., Table 3. Dots and squares are the calculated values, and the dashed lines are linear interpolations.

are fully consistent with the free energy results: the linear interpolation $\langle E_g \rangle = A + Bq$ of the calculated $\langle E_g \rangle$ as a function of charge gives $B \simeq 0$ in solution, whereas it is nonzero and negative for the gas-phase systems. Furthermore, the intercept at the origin A, corresponding to $\langle E_g \rangle$ for the neutral complex, is virtually the same in solution (1.58 eV) and in the gas phase (1.55 eV), which agrees well with the almost exactly superposing free energy profiles for $[EDTAH_2{\cdot}FeO]$ in gas phase and in solution at all values of ξ (Figure 4). The larger orbital gap in solution for the +2 complex is consistent with the higher barrier in solution (38 kJ mol^{-1}) relative to the gas phase (16 kJ mol^{-1}) and the smaller gap for the −2 complex with the lower barrier in solution (45 kJ mol^{-1} vs 57 kJ mol^{-1} in gas phase). This proves that the acceptor−donor energy difference is indeed the dominant factor determining the free energies of reaction and therefore the overall reactivity of the FeO^{2+} group. It also indicates that the reduced sensitivity of the reaction barrier on the complex charge in solution is a consequence of the reduced response of the energy gap between the acceptor $3\sigma^*$ and the donor orbital to the charge of the complex, compared to the gas phase.

In order to understand the origin of the smaller sensitivity of the orbital energy gap in solution, we analyzed the dipole response of the solvent to the charge of the complex. Under the assumption that the dominant contribution to the electrostatic field experienced by the FeO^{2+} group comes from the reorientation of the water dipoles under the influence of the charge of the complex, we can propose a simple model of the mechanism responsible for the stabilization (or destabilization) of the FeO^{2+} orbitals, in particular the $3\sigma^*$ orbital. For the positively charged complexes the water molecules in the nearest solvation shells will orient the negative end of their dipole vector toward the center of the complex (Fe). The dipoles will orient in the opposite direction for negatively charged complexes. In this model, the rearrangement of the water molecules is simply a charge-induced effect, created when a perturbing (point) charge is included in a responsive medium composed of an essentially random distribution of molecular dipoles.

To monitor the dependence of the solvent dipole orientation on the charge of the complex, we computed the thermally averaged angles θ of the dipole vector of each water molecule (defined by the centers of the negative and positive charges of each molecule) relative to the $Fe{-}O_{water}$ axis (Figure 8). These orientation angles were then averaged over the water molecules (i.e., the O atoms) in spherical shells centered at the Fe position, $\mathbf{R}_{Fe}$. The center of the positive charges of the i-th water molecule is given by

$$\boldsymbol{\mu}_i^+ = \sum_{I \in i} Z_I \mathbf{R}_I \quad (5)$$

where Z_I and $\mathbf{R}_I$ are the (pseudo) atomic charges and positions of the atoms belonging to the molecule. The position of the center of the negative charges was estimated from the positions of the centroids $\mathbf{c}_n$ of the set of maximally localized Wannier functions satisfying the Marzari−Vanderbilt localization condition:[121,122]

$$\boldsymbol{\mu}_i^- = -2 \sum_{n \in i} \mathbf{c}_n \quad (6)$$

$\mathbf{c}_n$ and $\mathbf{R}_I$ are measured relative to the center of mass of each water molecule. The sum in eq 6 is restricted to the set of Wannier centers associated to the i-th molecule, which can be determined by imposing a simple criterion based on the distance from the center of mass of the molecule.[123−125] The distribution of the average θ angles of the molecular dipoles within a spherical shell at a given distance from Fe is shown in Figure 8 as a function of the distance from Fe. The destabilization on the FeO^{2+} is largest when the dipole vector is oriented directly toward Fe, corresponding to θ = 0 in Figure 8. Values of θ approaching 180° will conversely stabilize the

dx.doi.org/10.1021/ja311144d | J. Am. Chem. Soc. 2013, 135, 8857−8867

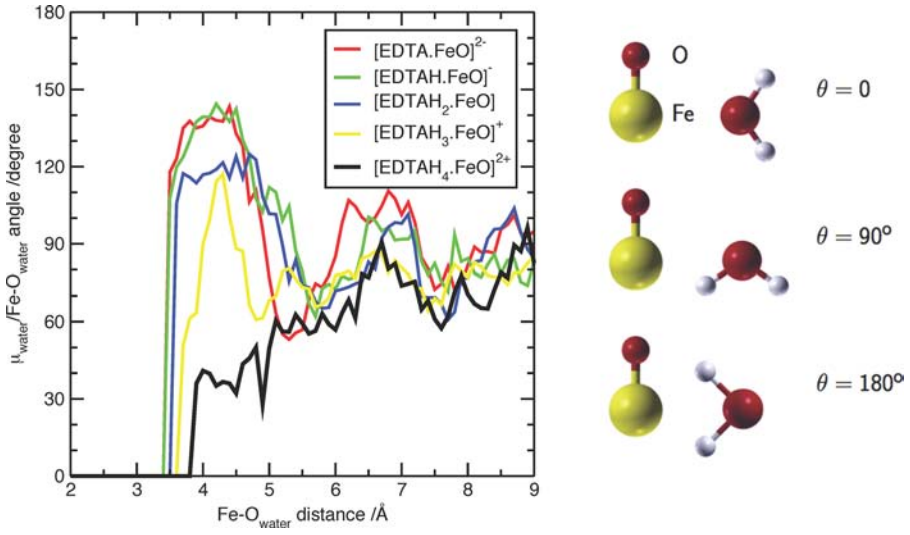

Figure 8. (Left) Effective orientation of the dipole vector of the solvent water molecules relative to the Fe−O_{water} vector, θ, as a function of the distance from the Fe atom. The θ value at a specific distance represents an average over all water molecules having their O atom in a spherical shell of thickness 0.1 Å centered on Fe, over 50 AIMD configurations spanning an overall simulation time of 5 ps. (Right) Models of the FeO^{2+}/H_2O dipole orientation, showing the convention for θ used in the plots.

FeO^{2+} orbital energies, because the positive end of the water dipole (roughly midway between the H−H axis) will now be oriented approximately toward Fe.

The results of this analysis are summarized in Table 4 in which we list the value of the dipole orientation for the shell of

Table 4. Average Orientation of the Water Dipole Moments in Degrees Relative to the Fe−O_{water} Vector[a]

complex	θ_0	θ_{max}	$\theta_{1st\ shell}$	θ_∞
$[EDTAH_4{\cdot}FeO]^{2+}$	36.00	40.94	39.58	82.58
$[EDTAH_3{\cdot}FeO]^{+}$	50.76	117.14	83.27	84.86
$[EDTAH_2{\cdot}FeO]$	105.64	121.54	111.51	84.37
$[EDTAH{\cdot}FeO]^{-}$	107.79	144.37	124.91	83.14
$[EDTA{\cdot}FeO]^{2-}$	117.90	143.31	133.24	94.88

[a] θ_0 is the value obtained from averaging over the first Fe-centered shell (corresponding to the first nonzero value of θ in the plots of Figure 8), θ_{max} is the value corresponding to the first maximum, $\theta_{1st\ shell}$ involves an average over shells up to the first minimum in each plot, and θ_∞ is the value at large distance (9 Å) from Fe.

water molecules at the shortest distance from Fe (θ_0), the dipole orientation at the first maximum (θ_{max}), the value averaged up to the first minimum in the plots of Figure 8 (θ_{min}), and the dipole orientation at large distance (9 Å) from Fe (θ_∞). As expected, the values of θ_0, θ_{max}, and θ_{min} tendentially increase as the charge of the complex varies from +2 to −2. This corresponds to a reorientation of the water molecules closer to the complex from the situation in which the negative end of the dipole vectors are oriented toward Fe ($\theta = 0°$) to the situation in which they point away from it ($\theta = 180°$). In practice, even in the two extreme sitations of the 2+ and −2 complexes, a deviation of 30−40° degrees is observed relative to these hypothetical limiting dipole orientations. This is expected, considering that other chemical or electrostatic interactions of the water molecules tend to randomize the distribution away from the ideal values $\theta = 0°$ and 180° to the average value of 90°. These interactions include H-bonds with other solvent molecules as well as with the carboxylate groups of the highly asymmetrical and mobile EDTA ligand. For the neutral complex, $[EDTAH_2{\cdot}FeO]$, the values of θ_0, θ_{max}, and θ_{min} are reasonably close to the value expected from a random distribution (90°). In this situation, the dipoles have little influence on the energy of the FeO^{2+} orbitals, and the free energies of reaction are then similar in gas phase and in solution (see Figure 4). For positively charged complexes the orbital energies (and, in particular the $3\sigma^*$ energy) are lowered by the charge of the complex, as is clear from the gas-phase energies shown in Figure 6, but the unfavorable orientation of the water dipoles cancels the charge-induced stabilization. The charge and dipole effects act again in opposite directions for negatively charged complexes, with a similar reciprocal cancellation. This explains the stability of the $3\sigma^*$ energy in solution and the much reduced sensitivity of the reaction barriers in solution on the complex charge. Finally, θ_∞ is very close to 90° for all systems, which shows that the dielectric screening of the charge of the complex is complete within ∼9 Å, and the dipoles are then randomly oriented at large distance from Fe, as in clean water.

To summarize our main argument: (1) The reactivity of an EDTA-chelated ferryl ion is importantly influenced by the charge of the ligand, and this effect can be interpreted in terms of a stabilization or destabilization of the acceptor $3\sigma^*$ orbital. Negative charges reduce the reactivity by destabilizing the $3\sigma^*$ orbital and reduce reactivity, and positive charges have the opposite effect. This is particularly evident in the gas-phase complexes (see Figure 7, squares, and compare to Figure 4, dashed lines). (2) The charge effect is damped in solution, where all complexes show comparable reactivities (Figure 4, continuous lines) and similar $3\sigma^*$ energies (Figure 7, dots). (3) The charge dampening in solution is a consequence of the dipole field induced in the local solvation structure by a charged solute: the complex with the highest positive charge (2+), which has the highest reactivity in solution, induces a reorientation of the water molecules in its vicinity in which all dipoles point their negative end approximately toward the complex center (Figure 8, black profile). In turn, this destabilizes the $3\sigma^*$ orbitals, canceling its charge-induced stabilization. Conversely, the −2 complex, whose reactivity in

dx.doi.org/10.1021/ja311144d | J. Am. Chem. Soc. 2013, 135, 8857−8867

the gas-phase is reduced by the large charge destabilization of the $3\sigma^*$ orbital, induces a rearrangement of the solvent water molecules and drives all closest dipoles to orient their positive end toward the complex center (Figure 8, red profile). In turn, this mechanism stabilizes the $3\sigma^*$ orbital and cancels the reduction of reactivity induced by the negative charge in the gas phase.

SUMMARY AND CONCLUSIONS

We have examined the reactivity of quintet FeO^{2+}/EDTA complexes as methane hydroxylation catalysts in aqueous solution and in the gas phase. By changing the protonation state of the EDTA ligand, we could study systematically the dependence of the H-abstraction from methane on the complex charge. A strong dependence is observed for the gas-phase systems, with free energies of reaction increasing from 16 to 57 kJ mol^{-1} as the charge varies between +2 and −2. This trend mirrors the dependence of the gas-phase reaction enthalpy on the charge, although the range of variation of the enthalpies is much larger (10−124 kJ mol^{-1}). This demonstrates the importance of entropic effects in determining the reaction barriers, which can be correlated to the relative "floppiness" of the EDTA ligand environment, particularly when the carboxylic arms are partially or fully deprotonated. In solution, the range of variation of the reaction free-energy barriers is much reduced (38−45 kJ mol^{-1}); effectively there is only a minor dependence of the reaction barriers on the charge. Besides, the neutral complex $[EDTAH_2{\cdot}FeO]$ yields the same free-energy reaction profile and barrier in gas phase and in solution. The consequence of these findings is that whereas the 2+ complex $EDTAH_4FeO^{2+}$ is more reactive in the gas phase than in solution (a common situation with charged reactants), the negative complexes $[EDTAH{\cdot}FeO]^-$ and $[EDTA{\cdot}FeO]^{2-}$ have lower reactivity in the gas phase (cf., Figure 4). We explain the damping of the reactivity dependence on the charge in solution as the result of two opposing effects: (1) the destabilization of the acceptor $3\sigma^*$ orbital of FeO^{2+} with increasing negative charge; and (2) the solute charge-induced reorientation of the solvent dipoles, which effectively stabilizes the $3\sigma^*$ orbital for negatively charged complexes and destabilizes it for positively charged ones. We have identified the difference in energy between the virtual $3\sigma^*$ orbital and the donor HOMO of methane as a suitable index of reactivity, both in the gas phase and in solution, which correlates directly with free-energy barriers of reaction.

These results provide a clear demonstration that not only (classical) electrostatic but also (quantum mechanical) electronic effects are important in determining the response of free-energy barriers to the presence of a solvent for hydroxylation processes and arguably also for a number of other classes of chemical reactions. The change in the orbital energies caused by the charge-induced reorientation of the solvent dipoles in the vicinity of the solute may in fact, as we have shown, completely cancel electrostatic effects and bring about unexpected changes in the reactivity in solution. We have identified, for the systems studied, suitable measures of the relative importance of orbital and electrostatic effects based on accurate electronic structure analysis and accounting for the real time evolution of solute and solvent molecules at room temperature. The energy of the substrate donor orbital can of course also be influenced by the presence of the solvent, particularly for charged species like negative Lewis bases, e.g., OH^- and halogen anions in S_N2 and E2 reactions. The donor orbital of such species will be stabilized in water solution, both by orbital interactions with empty states of surrounding water molecules and by the field created by the water dipoles, in much the same way described here for the $3\sigma^*$ acceptor orbital. This may have important implications for the preference of an S_N2 over an E2 reaction pathway.[126]

On the basis of these findings, it is also interesting to speculate if and how the reactivity of charged FeO^{2+}/EDTA systems as potential hydroxylation agents for hydrocarbon activation can further be enhanced in experimental conditions. For positively charged species, solvents with reduced polarity compared to water would likely bring the reactivity back to a level similar to the gas phase (which is predicted to be very high).[22] Suitable chemical modifications of the ligand (e.g., replacement of the carboxylic OH groups with aprotic groups) could also be envisaged, to avoid the tendency of the highly protonated (n = 3,4) FeO^{2+}/EDTA systems to transfer protons to solvent molecules, obviating the need to work at very low pH. For the negatively charged complexes, higher reactivity may be expected in the presence of strongly polar solvents with intermolecular interactions weaker than water. In this situation the charge-induced reorientation of the molecular dipoles will be more facile. Ideally, this could be accomplished using polar aprotic solvents, e.g., DMSO or $(CH_3)_2CO$. Effectively, we are looking for a hypothetical situation in which the slope of the $\langle E_g \rangle$ vs q dependence in Figure 7 is large and positive, which can potentially make the leftmost values of $\langle E_g \rangle$ comparable to those of the positively charged gas phase systems in the $q > 0$ part of the plot. This finding can have important implications for predicting and tuning the reactivity of FeO^{2+} complexes with charged ligands for organic oxidations in aqueous and nonaqueous environments, and we hope that our study may stimulate further experimental work in this direction.

ASSOCIATED CONTENT

Supporting Information

Atomic configurations from AIMD trajectories. This material is available free of charge via the Internet at http://pubs.acs.org.

AUTHOR INFORMATION

Corresponding Author

Leonardo.Bernasconi@stfc.ac.uk; E.J.Baerends@vu.nl

Notes

The authors declare no competing financial interest.

ACKNOWLEDGMENTS

This work was supported by EPSRC through a Service Level Agreement with STFC Scientific Computing Department and by the WCU (World Class University) program through the Korea Science and Engineering Foundation funded by the Ministry of Education, Science and Technology of the Republic of Korea (project no. R32-2008-000-10180-0). Computer resources were provided by The Netherlands' Scientific Research Council (NWO) through a grant from Stichting Nationale Computerfaciliteiten (NCF) and by STFC Rutherford Appleton Laboratory.

REFERENCES

(1) Hynes, J. T. *Annu. Rev. Phys. Chem.* **1985**, *36*, 573.
(2) Warshel, A. *J. Phys. Chem. A* **1979**, *83*, 3574.
(3) Warshel, A.; Russell, S. T. In *Molecular Dynamics and Protein Structure*; Polycrystal Book Service: Western Springs, IL, 1985.

(4) Chandrasekhar, J.; Smith, S. F.; Jorgensen, W. L. *J. Am. Chem. Soc.* **1985**, *107*, 154−163.
(5) Vayner, G. V.; Houk, K. N.; Jorgensen, W. L.; Brauman, J. I. *J. Am. Chem. Soc.* **2004**, *126*, 9054−9058.
(6) de Jong, G. T.; Bickelhaupt, F. M. *J. Chem. Theory Comput.* **2007**, *3*, 514−529.
(7) Rosta, E.; Kamerlin, S. C. L.; Warshel, A. *Biochemistry* **2008**, *47*, 3725−3735.
(8) van Bochove, M. A.; Bickelhaupt, F. M. *Eur. J. Org. Chem.* **2008**, 649−654.
(9) Kim, Y.; Cramer, C. J.; Truhlar, D. *J. Phys. Chem. A* **2009**, *113*, 9109.
(10) Liu, J.; Kelly, C. P.; Goren, A. C.; Marenich, A. V.; Cramer, C. J.; Truhlar, D. G.; Zhan, C.-G. *J. Chem. Theory Comput.* **2010**, *6*, 1109.
(11) Rosta, E.; Warshel, A. *J. Chem. Theory Comput.* **2012**, *8*, 3574.
(12) Savéant, J.-M. *Acc. Chem. Res.* **1993**, *26*, 455.
(13) Hammes-Schiffer, S. *Acc. Chem. Res.* **2001**, *34*, 273.
(14) Costentin, C.; Robert, M.; Savéant, J.-M. *Chem. Phys.* **2006**, *324*, 40.
(15) Costentin, C.; Robert, M.; Savéant, J.-M. *J. Am. Chem. Soc.* **2007**, *129*, 5870.
(16) Hammes-Schiffer, S.; Soudackov, A. V. *J. Phys. Chem. B* **2008**, *112*, 14108.
(17) Hammes-Schiffer, S.; Stuchebrukhov, A. A. *Chem. Rev.* **2010**, *110*, 6939.
(18) Englehardt, J. D.; Meeroff, D. E.; Echegoyen, L.; Deng, Y.; Raymo, F. M.; Shibata, T. *Environ. Sci. Technol.* **2007**, *41*, 270−276.
(19) Noradoun, C. E.; Cheng, I. F. *Environ. Sci. Technol.* **2005**, *39*, 7158−7163.
(20) Welch, K. D.; Davis, T. Z.; Aust, S. D. *Arch. Biochem. Biophys.* **2002**, *397*, 360−369.
(21) Gambardella, F.; Ganzeveld, I. J.; Winkelman, J. G. M.; Heeres, E. J. *Ind. Eng. Chem. Res.* **2005**, *44*, 8190−8198.
(22) Bernasconi, L.; Baerends, E. J. *Eur. J. Inorg. Chem.* **2008**, *2008*, 1672−1681.
(23) Bernasconi, L.; Baerends, E. J. *Inorg. Chem.* **2009**, *48*, 527−540.
(24) Belanzoni, P.; Bernasconi, L.; Baerends, E. J. *J. Phys. Chem. A* **2009**, *113*, 11926−11937.
(25) Bernasconi, L.; Belanzoni, P.; Baerends, E. J. *Phys. Chem. Chem. Phys.* **2011**, *13*, 15272−15282.
(26) Lippert, G.; Hutter, J.; Parrinello, M. *Mol. Phys.* **1997**, *92*, 477−487.
(27) VandeVondele, J.; Krack, M.; Mohamed, F.; Parrinello, M.; Chassaing, T.; Hutter, J. *Comput. Phys. Commun.* **2005**, *167*, 103−128.
(28) *Quickstep*, (2000−2007); http://cp2k.org (accessed March 30, 2011).
(29) Goedecker, S.; Teter, M.; Hutter, J. *Phys. Rev. B* **1996**, *54*, 1703−1710.
(30) Becke, A. *Phys. Rev. A* **1988**, *38*, 3098−3100.
(31) Lee, C.; Yang, W.; Parr, R. G. *Phys. Rev. B* **1988**, *37*, 785−789.
(32) Marx, D.; Hutter, J. *Modern Methods and Algorithms of Quantum Chemistry*; John von Neumann Institute for Computing: Julich, 2000; Vol. *1*; pp 301−449.
(33) Humphrey, W.; Dalke, A.; Schulten, K. *J. Mol. Graphics* **1996**, *14*, 33−38.
(34) Kokalj, A. *Comput. Mater. Sci.* **2003**, *28*, 155.
(35) Smith, W.; Forester, T. *J. Mol. Graphics* **1996**, *14*, 136.
(36) Berendsen, H. J. C.; Grigera, J. R.; Straatsma, T. P. *J. Phys. Chem.* **1987**, *91*, 6269.
(37) Bernasconi, L.; Baerends, E. J.; Sprik, M. *J. Phys. Chem. B* **2006**, *110*, 11444−11453.
(38) Carter, E. A.; Ciccotti, G.; Hynes, J. T.; Kapral, R. *Chem. Phys. Lett.* **1989**, *156*, 472.
(39) Sprik, M.; Ciccotti, G. *J. Chem. Phys.* **1998**, *109*, 7737.
(40) Babcock, G. T. *Proc. Natl. Acad. Sci. U.S.A.* **1999**, *96*, 12971−12973.
(41) Debrunner, P. G. *Hyperfine Interact.* **1990**, *53*, 21−36.
(42) Rutter, R.; Valentine, M.; Hendrich, M. P.; Hager, L. P.; Debrunner, P. G. *Biochemistry* **1983**, *22*, 4769−4774.
(43) Rutter, R.; Hager, L. P.; Dhonau, H.; Hendrich, M.; Valentine, M.; Debrunner, P. *Biochemistry* **1984**, *23*, 6809−6816.
(44) Price, J. C.; Barr, E. W.; Tirupati, B.; Bollinger, J. M., Jr.; Krebs, C. *Biochemistry* **2003**, *42*, 7497−7508.
(45) Price, J. C.; Barr, E. W.; Glass, T. E.; Krebs, C.; Bollinger, J. M., Jr. *J. Am. Chem. Soc.* **2003**, *125*, 13008−13009.
(46) Proshlyakov, D. A.; Henshaw, T. F.; Monterosso, G. R.; Ryle, M. J.; Hausinger, R. P. *J. Am. Chem. Soc.* **2004**, *126*, 1022−1023.
(47) Kryatov, S. V.; Rybak-Akimova, E. V.; Schindler, S. *Chem. Rev.* **2005**, *105*, 2175−2226.
(48) Solomon, E. I.; Brunold, T. C.; Davis, M. I.; Kemsley, J. N.; Lee, S.-K.; Lehnert, N.; Neese, F.; Skulan, A. J.; Yang, Y.-S.; Zhou, J. *Chem. Rev.* **2000**, *100*, 235−349.
(49) Lehnert, N.; Ho, R. Y. N.; Que, L., Jr.; Solomon, E. I. *J. Am. Chem. Soc.* **2001**, *123*, 8271−8290.
(50) Balcells, D.; Clot, E.; Eisenstein, O. *Chem. Rev.* **2010**, *110*, 749−823.
(51) Bray, W. C.; Gorin, M. H. *J. Am. Chem. Soc.* **1932**, *54*, 2124−2125.
(52) Groves, J. T.; Van Der Puy, M. *J. Am. Chem. Soc.* **1974**, *96*, 5274−5275.
(53) Groves, J. T.; McClusky, G. A. *J. Am. Chem. Soc.* **1976**, *98*, 859−861.
(54) Wardman, P.; Candeias, L. P. *Radiat. Res.* **1996**, *145*, 523−531.
(55) Dunford, H. B. *Coord. Chem. Rev.* **2002**, *233*, 311−318.
(56) Gozzo, F. *J. Mol. Catal. A: Chem.* **2001**, *171*, 1−22.
(57) Groves, J. T. *J. Inorg. Biochem.* **2006**, *100*, 434−447.
(58) Løgager, T.; Holcman, J.; Sehested, K.; Pedersen, T. *Inorg. Chem.* **1992**, *31*, 3523−3529.
(59) Pestovsky, O.; Bakac, A. *J. Am. Chem. Soc.* **2004**, *126*, 13757−13764.
(60) Pestovsky, O.; Stoian, S.; Bominaar, E. L.; Shan, X.; Münck, E.; Que, L., Jr.; Bakac, A. *Angew. Chem., Int. Ed.* **2005**, *44*, 6871−6874.
(61) Buda, F.; Ensing, B.; Gribnau, M. C. M.; Baerends, E. J. *Chem.—Eur. J.* **2001**, *7*, 2775−2783.
(62) Buda, F.; Ensing, B.; Gribnau, M. C. M.; Baerends, E. J. *Chem.—Eur. J.* **2003**, *9*, 3436−3444.
(63) Ensing, B.; Buda, F.; Blöchl, P.; Baerends, E. J. *Angew. Chem., Int. Ed.* **2001**, *40*, 2893−2895.
(64) Ensing, B.; Buda, F.; Blöchl, P.; Baerends, E. J. *Phys. Chem. Chem. Phys.* **2002**, *4*, 3619−3627.
(65) Ensing, B.; Buda, F.; Gribnau, M. C. M.; Baerends, E. J. *J. Am. Chem. Soc.* **2004**, *126*, 4355−4365.
(66) Louwerse, M. J.; Baerends, E. J. *Phys. Chem. Chem. Phys.* **2007**, *9*, 156−166.
(67) Eichhorn, E.; van der Ploeg, J. R.; Kertesz, M. A.; Leisinger, T. *J. Biol. Chem.* **1997**, *272*, 23031−23036.
(68) Shu, L.; Nesheim, J. C.; Kauffmann, K.; Muenck, E.; Lipscomb, J. D.; Que, L., Jr. *Science* **1997**, *275*, 515−518.
(69) Rosenzweig, A. C.; Nordlund, P.; Frederick, C. A.; Takahara, P. M. *Chemistry and Biology* **1995**, *2*, 409−418.
(70) Siegbahn, P. E. M.; Crabtree, R. H.; Nordlund, P. *J. Biol. Inorg. Chem.* **1998**, *3*, 314−317.
(71) Siegbahn, P. E. M. *Inorg. Chem.* **1999**, *38*, 2880−2889.
(72) Siegbahn, P. E. M. *J. Biol. Inorg. Chem.* **2001**, *6*, 27−45.
(73) Ambundo, E. A.; Friesner, R. A.; Lippard, S. J. *J. Am. Chem. Soc.* **2002**, *124*, 8770−8771.
(74) Guallar, V.; Gherman, B. J.; Lippard, S. J.; Friesner, R. A. *Curr. Opin. Chem. Biol.* **2002**, *6*, 236−242.
(75) Guallar, V.; Gherman, B. J.; Miller, W. H.; Lippard, S. J.; Friesner, R. A. *J. Am. Chem. Soc.* **2002**, *124*, 3377−3384.
(76) Merkx, M.; Kopp, D. A.; Sazinsky, M. H.; Blazyk, J. L.; Müller, J.; Lippard, S. J. *Angew. Chem., Int. Ed.* **2001**, *40*, 2782−2807.
(77) Kopp, D. A.; Lippard, S. J. *Curr. Opin. Chem. Biol.* **2002**, *6*, 568−576.
(78) Gherman, B. F.; Baik, M.-H.; Lippard, S. J.; Friesner, R. A. *J. Am. Chem. Soc.* **2004**, *126*, 2978−2990.
(79) Blazyk, J. L.; Lippard, S. J. *J. Biol. Chem.* **2004**, *279*, 5630−5640.
(80) Yoon, S.; Lippard, S. J. *J. Am. Chem. Soc.* **2004**, *126*, 2666−2667.

(81) Kovaleva, E. G.; Neibergall, M. B.; Chakrabarty, S.; Lipscomb, J. D. *Acc. Chem. Res.* **2007**, *40*, 475−483.
(82) Shteinman, A. A. *Russ. Chem. Rev.* **2008**, *77*, 945−966.
(83) Xue, G.; Wang, D.; Hont, R. D.; Fiedler, A. T.; Shan, X.; Munck, E.; Que, L., Jr. *Proc. Natl. Acad. Sci. U.S.A.* **2007**, *52*, 20713−20718.
(84) Wang, D.; Farquhar, E. R.; Stubna, A.; Münk, E.; Que, L., Jr. *Nature Chem.* **2009**, *1*, 145−150.
(85) Gopakumar, G.; Belanzoni, P.; Baerends, E. J. *Inorg. Chem.* (sumbitted).
(86) Tinberg, C. E.; Lippard, S. J. *Biochemistry* **2010**, *49*, 7902−7912.
(87) Friedle, S.; Reisner, E.; Lippard, S. J. *Chem. Soc. Rev.* **2010**, *39*, 2768−2779.
(88) Bukowski, M. R.; Koehntop, K. D.; Stubna, A.; Bominaar, E. L.; Halfen, J. A.; Münck, E.; Nam, W.; Que, L., Jr. *Science* **2005**, *310*, 1000−1002.
(89) Decker, A.; Rohde, J.-U.; Que, L., Jr.; Solomon, E. I. *J. Am. Chem. Soc.* **2004**, *126*, 5378−5379.
(90) Decker, A.; Clay, M. D.; Solomon, I. *J. Inorg. Biochem.* **2006**, *100*, 697−706.
(91) Kaizer, J.; Klinker, E. J.; Oh, N. Y.; Rohde, J.-U.; Song, W. J.; Stubna, A.; Kim, J.; Münck, E.; Nam, W.; Que, L., Jr. *J. Am. Chem. Soc.* **2003**, *126*, 472−473.
(92) Rohde, J.-U.; Que, L., Jr. *Angew. Chem., Int. Ed.* **2005**, *44*, 2255−2258.
(93) Rohde, J.-U.; In, J.-H.; Lim, M. H.; Brennessel, W. W.; Bukowski, M. R.; Stubna, A.; Münck, E.; Nam, W.; Que, L., Jr. *Science* **2003**, *299*, 1037−1039.
(94) Sastri, C. V.; Park, M. J.; Ohta, T.; Jackson, T. A.; Stubna, A.; Seo, M. S.; Lee, J.; Kim, J.; Kitagawa, T.; Münck, E.; Que, L., Jr.; Nam, W. *J. Am. Chem. Soc.* **2005**, *127*, 12494−12495.
(95) Shan, X.; Que, L., Jr. *J. Inorg. Biochem.* **2006**, *100*, 421−433.
(96) England, J.; Martinho, M.; Farquhar, E. R.; Frisch, J. R.; Bominaar, E. L.; Münck, E.; Que, L., Jr. *Angew. Chem., Int. Ed.* **2009**, *48*, 3622.
(97) England, J.; Guo, Y.; Farquhar, E. R.; Young, V. G., Jr.; Munck, E.; Que, L., Jr. *J. Am. Chem. Soc.* **2010**, *132*, 8635−8644.
(98) Cho, K.-B.; Shaik, S.; Nam, W. *ChemComm* **2010**, *46*, 4511−4513.
(99) Wong, S. D.; Bell, C. B., III; Liu, L. V.; Kwak, Y.; Solomon, E. I. *Angew. Chem., Int. Ed.* **2011**, *50*, 1−5.
(100) Crabtree, R. H. *Chem. Rev.* **1995**, *95*, 987−1007.
(101) Neidig, M. L.; Decker, A.; Choroba, O. W.; Huang, F.; Kanava, M.; Moran, G. R.; Spencer, J. B.; I.Solomon, , E. *Proc. Natl. Acad. Sci. U.S.A.* **2006**, *103*, 12966−12973.
(102) Hirao, H.; Kumar, D.; Que, L., Jr.; Shaik, S. *J. Am. Chem. Soc.* **2006**, *128*, 8590.
(103) Neese, F. *J. Inorg. Biochem.* **2006**, *100*, 716−726.
(104) Shaik, S.; Hirao, H.; Kumar, D. *Acc. Chem. Res.* **2007**, *40*, 532.
(105) Bernasconi, L.; Louwerse, M. J.; Baerends, E. J. *Eur. J. Inorg. Chem.* **2007**, *2007*, 3023−3033.
(106) Hirao, H.; Que, L., Jr.; Nam, W.; Shaik, S. *Chem.—Eur. J.* **2008**, *14*, 1740.
(107) Michel, C.; Baerends, E. J. *Inorg. Chem.* **2009**, *48*, 3628−3638.
(108) Janardanan, D.; Wang, Y.; Schyman, P.; Que, L., Jr.; Shaik, S. *Angew. Chem., Int. Ed.* **2010**, *49*, 3342−3345.
(109) Chen, H.; Lai, W.; Shaik, S. *J. Phys. Chem. Lett.* **2010**, *1*, 1533−1540.
(110) Geng, C.; Ye, S.; Neese, F. *Angew. Chem., Int. Ed.* **2010**, *49*, 1−6.
(111) Hegg, E. L.; Que, L., Jr. *Eur. J. Biochem.* **1997**, *250*, 625−629.
(112) Koehntop, K. D.; Emerson, J. P.; Que, L., Jr. *J. Biol. Inorg. Chem.* **2005**, *10*, 87−93.
(113) Makris, T. M.; von Koenig, K.; Schlichting, I.; Sligar, S. G. *J. Inorg. Biochem.* **2006**, *100*, 507−518.
(114) Gross, Z.; Nimri, S.; Barzilay, C. M.; Simkhovich, L. *J. Biol. Inorg. Chem.* **1997**, *2*, 492−506.
(115) Schöneboom, J. C.; Neese, F.; Thiel, W. *J. Am. Chem. Soc.* **2005**, *127*, 5840−5853.
(116) Shaik, S.; Kumar, D.; de Visser, S. P.; Altun, A.; Thiel, W. *Chem. Rev.* **2005**, *105*, 2279−2328.
(117) Seibig, S.; van Eldik, R. *Inorg. Chem.* **1997**, *36*, 4115−4120.
(118) Seibig, S.; van Eldik, R. *Eur. J. Inorg. Chem.* **1999**, *1999*, 447−454.
(119) Seibig, S.; van Eldik, R. *Inorg. React. Mech.* **1999**, *1*, 91−105.
(120) Costanzo, F.; Sulpizi, M.; Della Valle, R. G.; Sprik, M. *J. Chem. Phys.* **2011**, *134*, 244508.
(121) Marzari, N.; Vanderbilt, D. *Phys. Rev. B* **1997**, *56*, 12847−12865.
(122) Marzari, N.; Mostofi, A. A.; Yates, J. R.; Souza, I.; Vanderbilt, D. *Rev. Mod. Phys.* **2012**, *84*, 1419.
(123) Bernasconi, L.; Madden, P. A.; Wilson, M. *PhysChemComm* **2002**, *5*, 1−11.
(124) Bernasconi, L.; Blumberger, J.; Sprik, M.; Vuilleumier, R. *J. Chem. Phys.* **2004**, *121*, 11885.
(125) Molina, J. J.; Lectez, S.; Tazi, S.; Salanne, M.; Dufrêche, J.-F.; Roques, J.; Simoni, E.; Madden, P. A.; Turq, P. *J. Chem. Phys.* **2011**, *134*, 014511.
(126) Bickelhaupt, F. M.; Baerends, E. J.; Nibbering, N. M. M. *Chem.—Eur. J.* **1996**, *2*, 196−207.